Macrophage arginase-1 controls bacterial growth and pathology in hypoxic tuberculosis granulomas

María A. Duque-Correa[a], Anja A. Kühl[b], Paulo C. Rodriguez[c], Ulrike Zedler[a], Sandra Schommer-Leitner[a], Martin Rao[a], January Weiner III[a], Robert Hurwitz[d], Joseph E. Qualls[e,f], George A. Kosmiadi[g], Peter J. Murray[e,f], Stefan H. E. Kaufmann[a,1,2], and Stephen T. Reece[a,1,3]

[a]Department of Immunology and [d]Central Support Unit Biochemistry, Max Planck Institute for Infection Biology, 10117 Berlin, Germany; [b]Department of Immunopathology, Charité - University Medicine Berlin, 12200 Berlin, Germany; [c]Department of Microbiology, Stanley S. Scott Cancer Center, Louisiana State University Health Sciences Center, New Orleans, LA 70112; Departments of [e]Infectious Diseases and [f]Immunology, St. Jude Children's Research Hospital, Memphis, TN 38105; and [g]Immunology and Thoracic Surgery, Central Tuberculosis Research Institute, Moscow 107564, Russian Federation

Edited* by Carl F. Nathan, Weill Medical College of Cornell University, New York, NY, and approved August 21, 2014 (received for review May 13, 2014)

Lung granulomas develop upon *Mycobacterium tuberculosis* (*Mtb*) infection as a hallmark of human tuberculosis (TB). They are structured aggregates consisting mainly of *Mtb*-infected and -uninfected macrophages and *Mtb*-specific T cells. The production of NO by granuloma macrophages expressing nitric oxide synthase-2 (NOS2) via L-arginine and oxygen is a key protective mechanism against mycobacteria. Despite this protection, TB granulomas are often hypoxic, and bacterial killing via NOS2 in these conditions is likely suboptimal. Arginase-1 (Arg1) also metabolizes L-arginine but does not require oxygen as a substrate and has been shown to regulate NOS2 via substrate competition. However, in other infectious diseases in which granulomas occur, such as leishmaniasis and schistosomiasis, Arg1 plays additional roles such as T-cell regulation and tissue repair that are independent of NOS2 suppression. To address whether Arg1 could perform similar functions in hypoxic regions of TB granulomas, we used a TB murine granuloma model in which NOS2 is absent. Abrogation of Arg1 expression in macrophages in this setting resulted in exacerbated lung granuloma pathology and bacterial burden. Arg1 expression in hypoxic granuloma regions correlated with decreased T-cell proliferation, suggesting that Arg1 regulation of T-cell immunity is involved in disease control. Our data argue that Arg1 plays a central role in the control of TB when NOS2 is rendered ineffective by hypoxia.

The generic term "granuloma" describes an organized aggregate of immune and other cells formed in response to persistent stimuli of noninfectious or infectious origin (1–3). Granulomas develop in tuberculosis (TB), leprosy, schistosomiasis, and leishmaniasis and function to contain and sometimes destroy the etiologic agent (1–3). The precise role of granulomas in protection against TB remains elusive (1, 4–6). Although *Mycobacterium tuberculosis* (*Mtb*)-infected macrophages within granulomas are endowed with antimycobacterial defenses induced by the action of T cells, the long-term persistence of *Mtb* in the face of strong immune responses suggests that these mechanisms could be both evaded and harnessed by *Mtb* or that they function inefficiently in the granuloma environment (5, 7–9).

Two enzymes associated with key macrophage functions in TB granulomas are nitric oxide synthase-2 (NOS2) and arginase-1 (Arg1), which compete for the same substrate, L-arginine. The predominance of either enzyme spatially influences macrophage activation in different granuloma environments (8, 10–13). In the presence of oxygen, NOS2 metabolizes L-arginine into L-citrulline and nitric oxide (NO), which is associated with killing of intracellular pathogens (10, 13–15). Arg1 hydrolyzes L-arginine, producing urea and L-ornithine, which can be further metabolized to downstream products such as polyamines; Arg1 activity is associated with anti-inflammatory responses (10, 12, 13, 16). Knowledge of the immune and inflammatory functions of NOS2 and Arg1 comes largely from murine studies (12, 13). Production of NO and other reactive nitrogen intermediates (RNIs) is a key protective mechanism against *Mtb* infection in mice because NOS2-deficient ($Nos2^{-/-}$) mice infected with *Mtb* via aerosol and i.v. routes succumb to disease (17–21). Like NOS2, Arg1 is induced in murine and human macrophages upon infection with *Mtb*, and NOS2 activity in *Mtb* infection is hampered by Arg1 expression (22–24). Murine studies argue that Arg1 participates in dampening effective immunity against *Mtb*, because aerosol *Mtb*-infected mice that are deficient in macrophage-specific Arg1 have lower bacterial loads and smaller cellular infiltrates in the lungs than similarly infected WT mice (22). Moreover, *Mtb* aerosol infection of transgenic mice that overexpress IL-10 and IL-13 in macrophages results in increased pulmonary expression of Arg1, correlating with increased bacterial loads as compared with WT mice (25, 26). In these mouse models, Arg1 expression was linked to reduced production of RNIs, suggesting that L-arginine depletion by Arg1 suppresses NOS2 activity and, therefore, *Mtb* killing (22, 25). However, evidence from murine models of parasitic infection argues that Arg1 can have at least two other functions in addition to suppressing NOS2. First, macrophage Arg1 can reduce L-arginine availability to T cells, which are L-arginine auxotrophic, and can restrict local T-cell proliferation (10, 13, 27–29). Arginine restriction is an essential

Significance

Tuberculosis (TB) granulomas represent sites of both bacterial containment and tissue pathology. Macrophage killing of *Mycobacterium tuberculosis* (*Mtb*) in granulomas to contain infection must be regulated to prevent collateral tissue damage. Nitric oxide synthase-2 (NOS2) and arginase-1 (Arg1), macrophage enzymes metabolizing L-arginine, play key roles in this process. NOS2 produces reactive nitrogen intermediates to kill *Mtb*, whereas Arg1 regulates NOS2 activity via substrate competition. Arg1 activity could predominate in hypoxic regions of granulomas where NOS2 activity likely is suboptimal. Here we show that Arg1 plays a central role in restricting bacterial growth and restraining tissue damage within granulomas in TB and other chronic inflammatory diseases. These findings point to the modulation of Arg1 activity as a potential host-directed therapy for TB.

Author contributions: M.A.D.-C., S.H.E.K., and S.T.R. designed research; M.A.D.-C., A.A.K., U.Z., S.S.-L., M.R., R.H., and S.T.R. performed research; P.C.R., J.E.Q., G.A.K., and P.J.M. contributed new reagents/analytic tools; M.A.D.-C., A.A.K., M.R., J.W., R.H., and S.T.R. analyzed data; and M.A.D.-C., J.W., P.J.M., S.H.E.K., and S.T.R. wrote the paper.

The authors declare no conflict of interest.

*This Direct Submission article had a prearranged editor.

Freely available online through the PNAS open access option.

[1]S.H.E.K. and S.T.R. contributed equally to this work.

[2]To whom correspondence should be addressed. Email: kaufmann@mpiib-berlin.mpg.de.

[3]Present address: BioNTech RNA Pharmaceuticals GmbH, 55131 Mainz, Germany.

This article contains supporting information online at www.pnas.org/lookup/suppl/doi:10.1073/pnas.1408839111/-/DCSupplemental.

regulatory mechanism to restrain excessive T-cell responses in schistosomiasis granulomas, in which a Th2 response predominates and NOS2 expression is minimal (30). Moreover, depletion of L-arginine by Arg1 during *Leishmania* infection impairs Th1 responses required for parasite killing and subsequent lesion healing (31, 32). Second, products of L-arginine metabolism by Arg1 can affect parasite fitness directly. In particular, L-ornithine and polyamines promote the proliferation of *Leishmania* and *Plasmodium* parasites (33–35) but also directly block helminthic motility (36).

Because of the dominant NOS2 response during murine TB, determining the relative contributions of the Arg1 functions that are independent of NOS2 suppression in mice during *Mtb* infection remains technically challenging.

Here we devised a way to dissect the role of Arg1-expressing cells in TB lung granulomas in the absence of NOS2 by using the granuloma model of *Nos2*$^{-/-}$ mice dermally infected with *Mtb*. *Nos2*$^{-/-}$ mice dermally infected with *Mtb*, but not aerosol *Mtb*-infected *Nos2*$^{-/-}$ mice, recapitulate several features of TB granuloma pathology in humans, including hypoxia and caseation in the central regions of lung granulomas (37). We identified Arg1-expressing macrophages in hypoxic TB granulomas in the lungs of dermally *Mtb*-infected *Nos2*$^{-/-}$ mice that were analogous to TB lung granulomas in humans and nonhuman primates (NHPs) (11, 38). We demonstrate a critical role for Arg1-expressing macrophages in maintaining the ability of granulomas to control bacterial replication and to prevent pathology and provide evidence that this role involves spatial modulation of T-cell responses in specific granuloma microenvironments. Hence, our results indicate regulation by Arg1 in granulomas is important for balancing the control of *Mtb* growth and immunopathology during TB.

Results

Arg1 Is Expressed in TB Lung Granulomas of Infected *Nos2*$^{-/-}$ Mice and Is Associated with Necrosis. Arg1-expressing cells have been identified in TB lung granulomas in humans and NHPs (11, 38). Recently, we described the formation of human-like TB granulomas in *Nos2*$^{-/-}$ mice when *Mtb* bacilli disseminated to the lung via hematogenous spread from a primarily lymphatic focus after infection of the ear dermis (Fig. S1*A*) (37). Dermally *Mtb*-infected (hereafter referred to simply as "infected") *Nos2*$^{-/-}$ mice, but not WT mice, demonstrated culturable *Mtb* and mainly

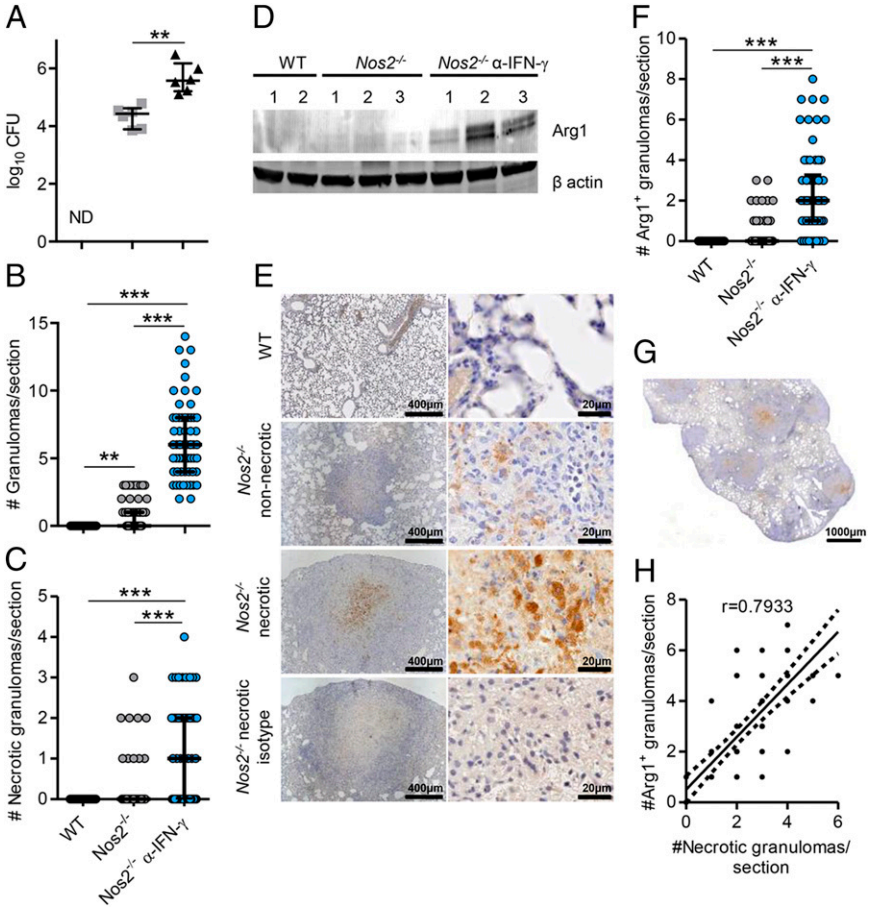

Fig. 1. Arg1 expression in lung granulomas of *Mtb*-infected *Nos2*$^{-/-}$ mice and association with necrosis. (*A*) Lung cfus from infected WT, *Nos2*$^{-/-}$, and IFN-γ–blocked *Nos2*$^{-/-}$ mice at day 56 p.i. Data are shown as median and interquartile range; $n = 6$ mice; $^{**}P = 0.0022$ (Mann–Whitney test). ND, not detectable. (*B* and *C*) Number of total granulomas (*B*) and number of necrotic granulomas (*C*) per lung section in infected WT ($n = 72$), *Nos2*$^{-/-}$ ($n = 66$), and IFN-γ–blocked *Nos2*$^{-/-}$ ($n = 62$) mice at day 56 p.i. Data are shown as median and interquartile range; $P < 0.0001$ (Gaussian approximation; Kruskal–Wallis test and Dunn's post test). (*D*) Arg1 expression in lung homogenates from infected WT, *Nos2*$^{-/-}$, and IFN-γ–blocked *Nos2*$^{-/-}$ mice at day 56 p.i. Protein (20 μg) was immunoblotted with anti-Arg1 and anti–β-actin. (*E*) IHC staining of lung tissue from infected WT and *Nos2*$^{-/-}$ mice with anti-Arg1 and isotype at day 56 p.i. (*F*) Number of Arg1^{+} granulomas per lung section in infected WT ($n = 72$), *Nos2*$^{-/-}$ ($n = 64$), and IFN-γ–blocked *Nos2*$^{-/-}$ ($n = 62$) mice at day 56 p.i. Data are shown as median and interquartile range. $P < 0.0001$ (Gaussian approximation; Kruskal–Wallis test and. Dunn's post test). (*G*) Representative Arg1 staining of a lung section from an IFN-γ–blocked *Nos2*$^{-/-}$ mouse at day 56 p.i. (*H*) Correlation between the number of necrotic and Arg1^{+} granulomas in the lungs of infected IFN-γ–blocked *Nos2*$^{-/-}$ mice. Spearman correlation; $P = 0.0001$. Data are representative of two independent experiments. $^{**}P < 0.005$; $^{***}P < 0.0005$.

nonnecrotizing granulomas, but also occasional necrotic granulomas, in the lungs at day 56 postinfection (p.i.) (Fig. 1 *A*–*C*) (37). When infected *Nos2*$^{-/-}$ mice were subjected to temporary antibody-mediated blocking of IFN-γ at days 14 and 21 p.i. (Fig. S1), they showed significantly increased bacterial burden and numbers of granulomas in the lungs at day 56 p.i., with a greater proportion demonstrating hypoxia and central caseation, classical features of human granuloma pathology (Fig. 1 *A*–*C*) (37). We investigated whether Arg1 was expressed in lung granulomas in this model. First, we evaluated whether Arg1 expression was increased in the lungs of infected mice. Using immunoblotting (Fig. 1*D*), we detected increased expression of Arg1 in the lung of infected *Nos2*$^{-/-}$ and IFN-γ–blocked *Nos2*$^{-/-}$ mice as compared with WT mice at day 56 p.i.

We identified Arg1^{+} cells occasionally in nonnecrotizing granulomas and consistently in caseous necrotic granulomas in infected *Nos2*$^{-/-}$ mice (Fig. 1*E* and Fig. S2 *A* and *B*). Arg1 was abundant in the region around the necrotic core of the granulomas but was undetectable in lungs of infected WT mice (Fig. 1*E* and Fig. S2 *A* and *B*). Furthermore, infected IFN-γ–blocked *Nos2*$^{-/-}$ mice had significantly elevated numbers of Arg1^{+} lung granulomas as compared with untreated infected *Nos2*$^{-/-}$ mice (Fig. 1 *F* and *G*). Analysis using Spearman's correlation coefficient demonstrated a significant positive association ($r = 0.7933$) between the numbers of necrotic and Arg1^{+} granulomas in the lungs of infected IFN-γ–blocked *Nos2*$^{-/-}$ mice (Fig. 1*H*), suggesting Arg1 expression correlated with exacerbated lung granuloma pathology.

Previously, hypoxic [pimonidazole-positive (PIMO^{+})] cells were identified in regions surrounding the necrotic center of TB lung granulomas in infected *Nos2*$^{-/-}$ mice (37), the region where Arg1^{+} cells are located. Because hypoxic conditions are well-known inducers of Arg1 in macrophages (39, 40), we investigated whether Arg1^{+} cells stained for PIMO. PIMO enters cells in tissues with low O_2 partial pressure and forms adducts with thiol groups within proteins; these adducts can be detected by immunohistochemistry (IHC) (Fig. S3). By comparing Arg1 and PIMO staining in strictly consecutive sections from the same granuloma, we demonstrated that cells expressing Arg1 did not themselves stain for PIMO but located proximally to hypoxic cells localized at the necrotic center of caseous granulomas in *Nos2*$^{-/-}$ mice (Fig. S3). Taken together, our findings demonstrate Arg1 is expressed in TB lung granulomas of infected *Nos2*$^{-/-}$ mice, particularly within the regions encircling the central necrotic core of caseous hypoxic granulomas.

Macrophages Are the Main Cell Type Expressing Arg1 in TB Lung Granulomas of Infected *Nos2*$^{-/-}$ Mice. To identify which cells expressed Arg1, we stained sections of lungs of infected *Nos2*$^{-/-}$ mice at day 56 p.i. with antibodies specific for the macrophage marker CD68 and Arg1 using immunofluorescence (IF). Cells expressing Arg1 in both nonnecrotic and necrotic granulomas in lungs of infected *Nos2*$^{-/-}$ mice coexpressed CD68 (Fig. S4*A*). In some caseous granulomas, Arg1 expression did not colocalize precisely with CD68 in the necrotic core (Fig. S4*A*). Because these regions are largely acellular, Arg1 may also be extracellular in this pathophysiological context.

To characterize the phenotype of Arg1-expressing cells further, cells were isolated from lungs of infected *Nos2*$^{-/-}$ and IFN-γ–blocked *Nos2*$^{-/-}$ mice and were stained with antibodies for neutrophil, inflammatory macrophage, monocyte, alveolar macrophage, and dendritic cell surface markers and for intracellular Arg1 (Fig. 2*A* and Fig. S4 *B* and *D*). Notably, we observed a significant decrease in the percentages of neutrophils, alveolar macrophages, and monocytes in lungs of infected IFN-γ–blocked *Nos2*$^{-/-}$ mice as compared with infected *Nos2*$^{-/-}$ mice (Fig. 2*A*). Supporting our IF data (Fig. S4*A*), inflammatory macrophages were the main cellular population expressing Arg1 in the lungs of infected *Nos2*$^{-/-}$ mice and IFN-γ–blocked *Nos2*$^{-/-}$ mice. Small percentages of neutrophils and monocytes were positive

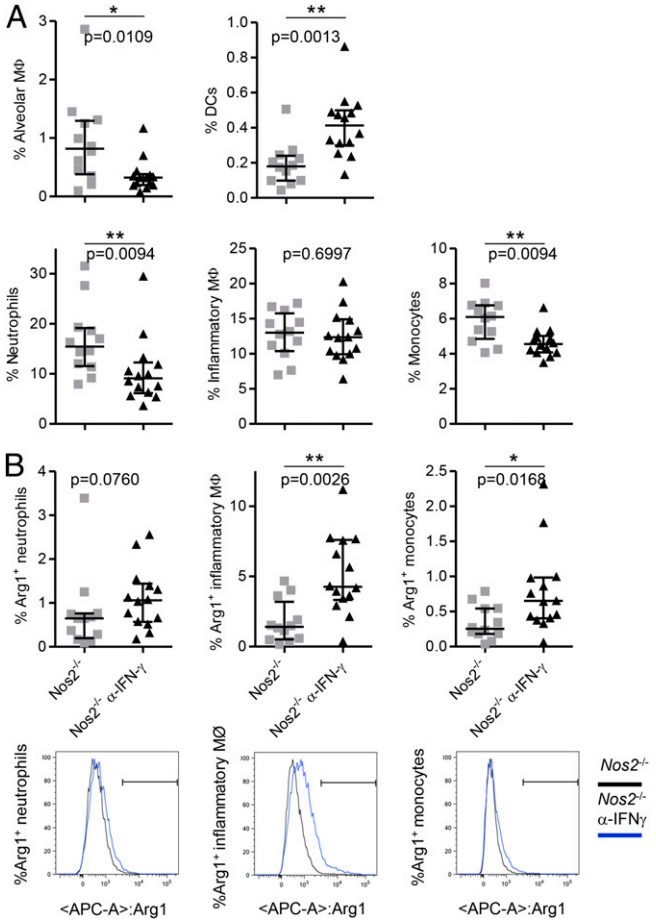

Fig. 2. Macrophages are the main cell type expressing Arg1 in lungs from *Mtb*-infected *Nos2*$^{-/-}$ mice. (*A*) Single-cell lung suspensions prepared at day 56 p.i. were analyzed by flow cytometry to detect the frequency of the indicated immune cell populations in the lungs of infected *Nos2*$^{-/-}$ and IFN-γ–blocked *Nos2*$^{-/-}$ mice. (*B*) Percentages of Arg1^{+} cells in neutrophils, inflammatory macrophages, and monocytes in lungs of infected *Nos2*$^{-/-}$ and IFN-γ–blocked *Nos2*$^{-/-}$ mice at day 56 p.i. Histograms show Arg1 expression in neutrophils, inflammatory macrophages, and monocytes. The black line depicts *Nos2*$^{-/-}$ mice ($n = 12$), and the blue line depicts IFN-γ–blocked *Nos2*$^{-/-}$ mice ($n = 14$). Data are shown as median and interquartile range. Mann–Whitney test. Data are representative of two independent experiments. $^{*}P < 0.05$; $^{**}P < 0.01$.

for Arg1 also (Fig. 2*B* and Fig. S4 *C* and *D*). These data suggest recruited monocytes are induced to express Arg1 in the lung and later differentiate into inflammatory macrophages while continuously expressing Arg1. Moreover, because murine neutrophils do not express Arg1, it is possible that Arg1^{+} neutrophils have phagocytosed apoptotic Arg1-expressing macrophages or internalized the enzyme from the extracellular milieu. Although arginases are intracellular enzymes, they can be released into the extracellular environment when the cellular membrane is breached and retain activity upon release (41). The high level of macrophage necrosis in caseous granulomas in infected *Nos2*$^{-/-}$ mice could explain the observation of extracellular Arg1 in our model. To confirm our enzyme-localization data in human tissue, we stained lung sections from patients with cavitary TB and tuberculoma. Based on morphology, Arg1^{+} cells were classified as alveolar macrophages (Fig. S5*A*), multinucleated giant cells (Fig. S5*B*), and tissue macrophages (Fig. S5 *C* and *D*), confirming a recent report on Arg1 expression in human TB (38). Together, these data indicate macrophages are the main cell type expressing Arg1 in TB lung granulomas.

Arg1 Restricts L-Arginine Concentrations and Increases the Abundance of Polyamines in the Lungs of Infected *Nos2*$^{-/-}$ Mice. Arginases hydrolyze L-arginine to produce urea and L-ornithine, which then can be metabolized further to polyamines (spermine, spermidine, and putrescine), which are important regulators of cellular proliferation and immunosuppression (10, 13, 42). Arginase activity also can deplete L-arginine, restricting antigen-specific T-cell proliferation (10, 13, 42). To dissect the relative contribution of these two pathways in TB in the absence of NOS2, we first quantified arginase activity and L-arginine metabolites in the lungs of infected mice. Arginase activity in the lungs of infected *Nos2*$^{-/-}$ and IFN-γ–blocked *Nos2*$^{-/-}$ mice (Fig. 3*A*) was associated with a reduction in total L-arginine concentrations and increased amounts of L-ornithine, putrescine, and spermidine (Fig. 3*B*). Thus, the elevated expression and activity of Arg1 in the lungs of infected *Nos2*$^{-/-}$ and IFN-γ–blocked *Nos2*$^{-/-}$ mice resulted in a local increase in polyamine concentrations and depletion of L-arginine during TB. We next assessed the relative importance of the ornithine-production versus arginine-depletion pathways in TB.

Metabolites Derived from L-Arginine Do Not Affect *Mtb* Growth in Vitro. The exogenous supply of metabolites derived from L-arginine supports the proliferation of protozoan parasites such as *Leishmania* and *Plasmodium* (33–35). In contrast, Arg1-generated ornithine and polyamines are directly antihelminthic (36). We next addressed whether a similar addition of these metabolites affected proliferation of *Mtb* in vitro. We therefore cultured *Mtb* strain H37Rv in Sauton's minimal medium supplemented with concentrations of L-arginine, L-ornithine, putrescine, spermidine, and spermine and followed bacterial growth for 1, 2, 4, and 7 d of culture. We did not find that these metabolites had any influence on *Mtb* growth in vitro (Fig. S6). These data suggest that the observed decrease in detectable L-arginine and increase in L-ornithine, putrescine, and spermidine in the lungs of infected IFN-γ–blocked *Nos2*$^{-/-}$ mice was unlikely to affect *Mtb* burden in the lung.

Abrogation of Macrophage Arg1 Exacerbates *Mtb* Growth and Pathology in TB Lung Granulomas. Having ruled out direct effects of ornithine or polyamines on *Mtb* growth, we next turned to a genetic system to evaluate the consequences of Arg1 deletion on immune cells and TB granuloma maintenance. To this end, we created mice lacking Arg1 in macrophages on a complete NOS2-deficient background [*Arg1*$^{flox/flox}$; Tie2-Cre; *Nos2*$^{-/-}$ mice, hereafter referred to as "*Arg1-Nos2* double knockout (DKO) mice"]. Although the Tie2-Cre deleter is found in all hematopoietic and endothelial cells, Arg1 is expressed mainly by macrophages in our model, and thus *Arg1-Nos2* DKO mice allow us to delete Arg1 specifically in macrophages (Fig. S1*B*) (22). *Arg1*$^{flox/flox}$; Tie2-Cre mice were not used here, because they do not represent an appropriate control for the NOS2-deficient granuloma model. *Mtb* infection of *Arg1*$^{flox/flox}$; Tie2-Cre mice has been reported previously (22).

Histological analyses of *Arg1-Nos2* DKO mice dermally infected with *Mtb* demonstrated striking granuloma enlargement as compared with *Nos2*$^{-/-}$ mice at day 56 p.i. (Fig. 4*A*). In addition, we observed a significant increase in both the total number of granulomas and the number of necrotic granulomas in the lungs of infected *Arg1-Nos2* DKO mice in comparison with infected *Nos2*$^{-/-}$ mice (Fig. 4*B*), and these increases were linked with an increase in the total bacterial burden in the lung (Fig. 4*C*). Based on the results from the temporary blocking of IFN-γ in infected *Nos2*$^{-/-}$ mice, we predicted that IFN-γ–blocked infected *Arg1-Nos2* DKO mice would show exacerbated pathology and bacterial growth as compared with infected nonblocked *Arg1-Nos2* DKO mice. When we subjected infected *Arg1-Nos2* DKO mice to IFN-γ blocking, we observed extreme proteolysis in the lungs, elevated numbers of necrotic granulomas, and exceedingly high bacterial counts at day 56 p.i. (Fig. S7). This extensive pathology warranted cessation of the experiments according to veterinary guidelines to keep animal suffering within reasonable limits. Taken together, our findings indicate that Arg1 abrogation affects the ability to control *Mtb* growth and pathology in granulomas in the lung.

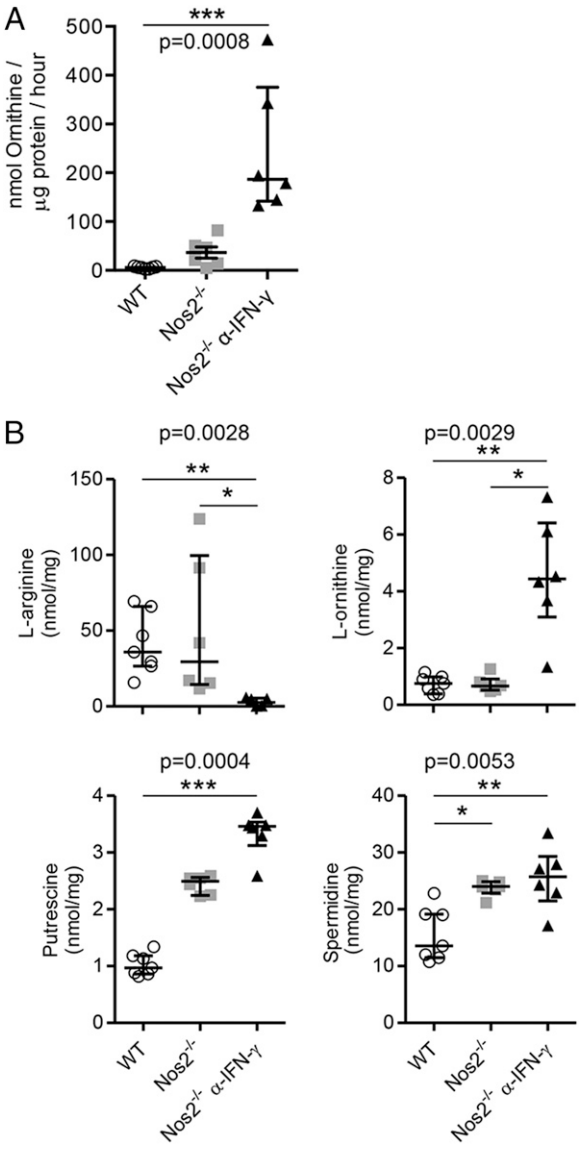

Fig. 3. Arg1 metabolizes L-arginine, producing L-ornithine and polyamines in lungs of *Mtb*-infected *Nos2*$^{-/-}$ mice. (*A*) Arginase activity measured by the conversion of L-arginine into L-ornithine. (*B*) Amounts of L-arginine, L-ornithine, putrescine, and spermidine detected by HPLC in lung homogenates of infected WT ($n = 7$), *Nos2*$^{-/-}$ ($n = 6$), and IFN-γ–blocked *Nos2*$^{-/-}$ ($n = 6$) mice at day 56 p.i. Data are shown as median and interquartile range. Kruskal–Wallis test and Dunn's post test. Data are representative of two independent experiments. *$P < 0.05$; **$P < 0.005$; ***$P < 0.0005$.

Arg1-Expressing Macrophages Correlate with Restrained T-Cell Responses in TB Lung Granulomas. We hypothesized that the increased granuloma pathology and inability to control *Mtb* growth in the lungs of infected *Arg1-Nos2* DKO mice could be associated with a role of Arg1 in blocking T-cell proliferation in granuloma microenvironments. Therefore, we first determined whether the presence of Arg1^{+} cells correlated with reduced T-cell proliferation by staining TB lung granulomas for Arg1, CD3ε to designate T cells, and Ki-67, an established marker of cellular proliferation. T cells stained for CD3ε lacked Ki-67 expression when localized

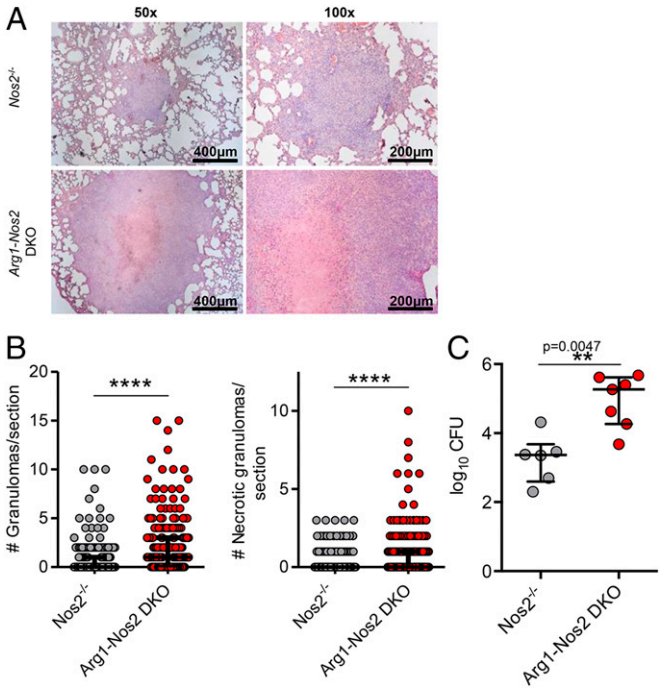

Fig. 4. Abrogation of Arg1 exacerbates *Mtb* growth and pathology in TB lung granulomas. (*A*) H&E staining of lung tissue from infected *Nos2*$^{-/-}$ and *Arg1-Nos2* DKO mice at day 56 p.i. (*B*) Number of total and necrotic granulomas per lung section in infected *Nos2*$^{-/-}$ (n = 259) and *Arg1-Nos2* DKO (n = 196) mice on day 56 p.i. Data are shown as median and interquartile range. ****P < 0.0001 (Gaussian approximation; Mann–Whitney test). (*C*) Lung cfus from infected *Nos2*$^{-/-}$ (n = 6) and *Arg1-Nos2* DKO (n = 7) mice at day 56 p.i. Data are shown as median and interquartile range. Mann–Whitney test. Data are representative of three independent experiments.

in the regions surrounding the necrotic core of granulomas from infected *Nos2*$^{-/-}$ mice where Arg1$^+$ macrophages were located (Fig. S8). In contrast, Ki-67 was expressed by T cells of nonnecrotizing granulomas and in areas distant from the necrotic center, where Arg1$^+$ macrophages were fewer (Fig. S8). Strikingly, T cells surrounding the necrotic regions of granulomas from infected *Arg1-Nos2* DKO mice were positive for Ki-67 (Fig. S8).

To quantify the effects of Arg1$^+$ cells on T-cell proliferation in TB lung granulomas, we acquired images from the center of the granuloma (defined as region 1), subsequently moving sequentially through regions 2–4 toward the outer limits of the granuloma (Fig. 5*A*). Numbers of Ki-67$^+$ cells and the area (in square pixels) of Arg1$^+$ staining were quantified from each image. We performed this analysis on IHC-stained sections, because the autofluorescence inherent to lung specimens complicated quantitative measurements using IF-stained sections. Moreover, we included sections from lungs of both infected *Nos2*$^{-/-}$ and IFN-γ– *Nos2*$^{-/-}$ mice because IFN-γ–blocked *Nos2*$^{-/-}$ mice presented higher numbers of total, necrotic, and Arg1$^+$ lung granulomas (Fig. 1), and inclusion of these mice allowed us to increase the sample size (Fig. S1*C*). This analysis revealed a highly significant negative correlation between the number of Ki-67$^+$ cells and the area (in square pixels) of Arg1$^+$ staining (r = –0.49, P < 0.0001) in granulomas of infected *Nos2*$^{-/-}$ and IFN-γ–blocked *Nos2*$^{-/-}$ mice (Fig. 5*B*). Using the same sequential image analysis and a mixed-effect linear regression model, we next evaluated differences in the gradient of Ki-67$^+$ cells from the center to the outer limit of the granuloma (regions 1–4) between granuloma types (nonnecrotic or necrotic) and in the presence or absence of Arg1 expression (i.e., *Nos2*$^{-/-}$ and *Arg1-Nos2* DKO mice). In necrotic TB lung granulomas the slope of the gradient of Ki-67$^+$ cells through regions 1–4 was steeper when Arg1 was present (i.e., in infected *Nos2*$^{-/-}$ and IFN-γ–blocked *Nos2*$^{-/-}$ mice) than when Arg1 was absent (i.e., in infected *Arg1-Nos2* DKO mice) (Fig. 5*C* and Fig. S9*C*). This difference was indicated by a significant interaction between granuloma region and Arg1 presence (P < 0.05) and between granuloma region and granuloma type (P < 0.02). Moreover, in a separate analysis of the two granuloma types, the interaction between granuloma region and Arg1 presence was significant for necrotic granulomas (P < 0.02) but not for nonnecrotic granulomas (P = 0.35) (Fig. 5*C* and Fig. S9). Thus, we conclude Arg1 influenced the gradient of Ki-67$^+$ cells in necrotic TB lung granulomas, indicating that the presence of Arg1-expressing macrophages affects T-cell proliferation. Taken together, these results suggest that Arg1-expressing macrophages control *Mtb* growth and pathology and that this control is associated with the ability to regulate the proliferative capacity of colocalizing T cells in central hypoxic regions of TB granulomas.

Discussion

Histological studies of lung samples from TB patients indicate that granuloma architecture has a critical role in orchestrating immune responses (6, 43, 44). Proliferative activity and cytokine production are observed mainly at the peripheral leukocyte infiltrate outside the necrotic center and the fibrous wall of the granuloma rather than at the interface between the inner cellular layer and necrotic tissue (6, 43). Although the granulomas in our model did not demonstrate extensive fibrosis, the observations in human TB are in line with increased T-cell proliferative capacity at sites more distant from the necrotic granulomatous center in the infected *Nos2*$^{-/-}$ model. In the central region, expansion of the necrotic zone at the expense of surrounding cells results from cytokine-mediated toxicity and the release of proteolytic enzymes by macrophages (2, 44–46). Therefore, control of immune responses at this site by Arg1 could reduce development and expansion of necrosis during TB. Together with the recent data showing a spatial distribution of Arg1-expressing macrophages in TB granulomas of NHPs (11), our data suggest that Arg1-expressing macrophages exert immunosuppressive functions in microenvironments in granulomas that are required for protection against disease.

In this study, we aimed at addressing the functional properties of Arg1 during TB that are independent of its ability to control NO production via NOS2 by competing for L-arginine, the shared substrate for both enzymes. To do so, we used a murine model of TB in which dermal *Mtb* infection of *Nos2*$^{-/-}$ mice results in the hematogenous spread of infection to the lung. There, granulomas demonstrate hypoxia and central necrosis, canonical properties of human granulomas that are typically not seen after conventional aerosol or i.v. infection of mice. Using this model, we identified Arg1 expression in lung granulomas analogous to those in TB patients and in NHP models of TB (11, 38). Arg1-expressing cells surrounded the necrotic, hypoxic center of caseous granulomas, suggesting the hypoxic environment in this region potentially contributes to Arg1 induction (39, 40, 47–49). As reported in human and NHP TB granulomas (11, 38), inflammatory macrophages were the major cellular population expressing Arg1 in TB lung granulomas of *Nos2*$^{-/-}$ mice. This observation contrasts with the recent finding that in aerosol *Mtb*-infected *Nos2*$^{-/-}$ mice CD11b$^+$ myeloid-derived suppressor cells (MDSCs) expressing high levels of Arg1 are located at the edges of necrotic lung lesions in which neutrophils and MDSCs are thought to be the main drivers of lung necrosis (50). Differences in bacterial burden in the lung upon aerosol and dermal infection would affect the kinetics of inflammatory cellular influx into the lung, which subsequently determines the ultimate architecture and structure of the lesions (37, 50). More specifically, the lower bacterial counts (10^4 cfus) at early time points (day 30 p.i.) in our model, as compared with aerosol-infected mice (10^6 cfus), could allow the development of more stratified granulomas

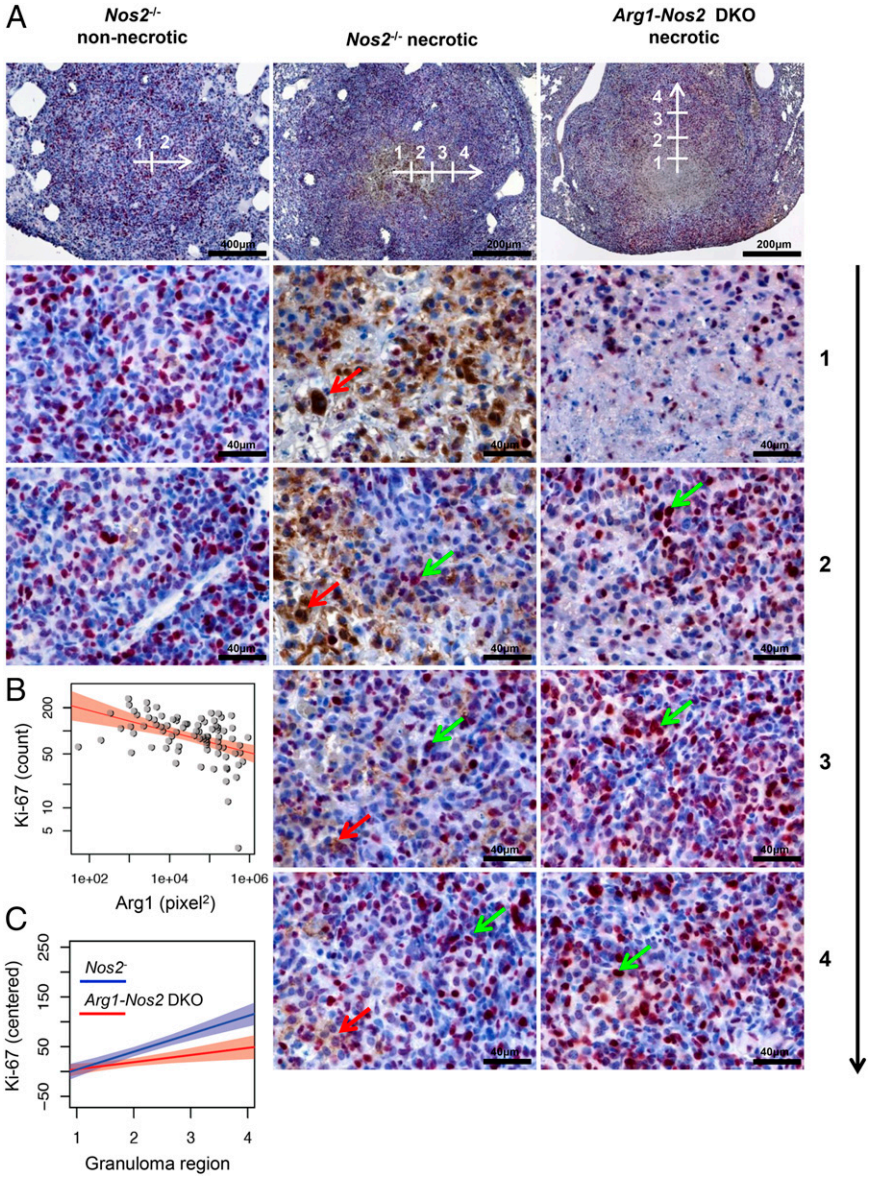

Fig. 5. Proximity of Arg1$^+$ cells affects T-cell proliferation in microenvironments within granulomas. (*A*) Representative nonnecrotic and necrotic granulomas from infected *Nos2*$^{-/-}$ and *Arg1-Nos2* DKO mice at day 56 p.i. stained with anti-Arg1 (brown staining, red arrow) and anti-Ki67 (fuchsia staining, green arrow). White arrow and numeration on pictures taken at 50× and 100× magnification show the position where pictures at 400× magnification were acquired starting from the center (1) and moving toward the outer limits of the granuloma (2–4). (*B*) Correlation between area (in square pixels) of Arg1$^+$ staining and the number of Ki-67$^+$ cells quantified in granulomas from infected *Nos2*$^{-/-}$ and IFN-γ–blocked *Nos2*$^{-/-}$ mice at day 56 p.i. The red lines show the log-linear regression fit for data points with positive value; the pink area denotes the 95% confidence band. The fitted regression coefficient is significant with $P < 0.0001$ ($r^2 = 0.2$; Spearman correlation) ($n = 134$ pictures from regions of 50 granulomas). $P < 0.00001$ ($r = -0.49$). (*C*) Linear regression of gradient of numbers of Ki-67$^+$ cells in necrotic granulomas from infected *Nos2*$^{-/-}$ and IFN-γ–blocked *Nos2*$^{-/-}$ mice (blue line) and *Arg1-Nos2* DKO mice (red lines) at day 56 p.i. Lines correspond to linear fits of centered Ki-67$^+$ cells' values on a separate granuloma region for each of the two subgroups. Shaded areas show corresponding 95% confidence bands. The interaction between mouse strain and granuloma region is significant ($P < 0.02$) as tested by a separate complete mixed-effects model.

(37) in which the proportion of neutrophils is lower and necrosis is caused mainly by the death of highly infected macrophages from cytokine-mediated toxicity. These granulomas are more representative of the typical granulomas seen in experimental TB in NHPs, which in turn are considered the models most representative of the human pathology (51). A key difference in our study and NHP studies is the expression of both Arg1 and NOS2 in macrophages in the latter. In NHP TB granulomas, the NOS2:Arg1 ratio was highest in central regions, where bacterial burden is maximal (11). Although Mattila et al. (11) observed that NOS2 is active in these areas, the uncontrolled bacterial proliferation suggests that hypoxia indeed limits NOS2 efficiency and that additional functions of Arg1, independent of NOS2 control, could come into play.

In our model, Arg1 expression correlated with necrosis and was associated with bacterial burden in the lung. Our findings agree with previous observations showing increased Arg1 mRNA expression and Arg1 activity over the course of aerosol *Mtb* infection and its association with augmented bacterial burden in murine lungs (22, 26, 50). Using the aerosol *Mtb* challenge of macrophage Arg1-deficient mice, El Kasmi et al. (22) demonstrated improved control of *Mtb* in the lung. In contrast, abrogation of Arg1 and NOS2 in our model resulted in exacerbated

granuloma pathology and bacterial growth as compared with NOS2 deficiency alone. These data can be reconciled by additional functions of Arg1 in the absence of NOS2, in a system where Arg1 is expressed spatially in an organized granuloma environment. We did not detect a direct effect of metabolites derived from L-arginine on *Mtb* growth in vitro, suggesting that Arg1 does not restrict *Mtb* growth directly. However, these metabolites may require additional tissue-specific factors to exert this effect.

Uncontrolled T-cell responses to mycobacterial antigens could contribute to immunopathology driven by lung tissue damage during TB. For instance, patients coinfected with HIV and *Mtb*, who present low counts of $CD4^+$ T cells, lack caseating granulomas (46, 52). Immune reconstitution in these patients by antiretroviral therapy results in the increased development of lung pathology associated with TB (46, 52). We identified increased numbers of proliferating T cells in areas around the necrotic core of granulomas in absence of Arg1 expression, suggesting that Arg1-expressing macrophages would be ideally positioned to contribute to the local regulation of T-cell proliferation in this microenvironment, which in TB lung granulomas is a key battlefield between host and microbe. A caveat of alternative approaches for studying the effects of Arg1 on T-cell proliferation and the activation of lung T cells is that the granuloma architecture must be destroyed to obtain the cells. Thus, we consider histological analysis to be more informative about the local effects of Arg1. Arg1 activity in the lung from infected *Nos2*$^{-/-}$ mice resulted in local depletion of L-arginine and production of L-ornithine and polyamines. Both the anti-inflammatory effects of polyamines and the depletion of L-arginine from the extracellular milieu could be responsible for suppressed T-cell responses. Moreover, additional environmental features of the granuloma caseous center, such as oxygen and glucose gradients, could contribute to the suppression of T-cell proliferation.

Our results agree with similar suppressive roles of Arg1-expressing macrophages in other chronic infectious diseases. During infections with the intracellular parasites *Leishmania sp*., *Schistosoma mansoni*, and *Trypanosoma sp.*, Arg1 expression/activity was induced concomitantly with increasing parasite load (31, 53–55). Moreover, Arg1-expressing cells accumulate in and around *S. mansoni* granulomas (30, 55, 56) and in skin lesions from patients who have cutaneous leishmaniasis (57); these lesions often are necrotic and hypoxic (58, 59). In murine *S. mansoni* infection, Arg1-expressing macrophages restrain Th2 cytokine-driven inflammation and fibrosis (30, 60). Notably, during *Leishmania* infection in mice, Arg1 contributes to the failure to heal persistent lesions, which is a consequence of impaired T-cell responses to *L. major* resulting from local depletion of L-arginine by arginase (32). Taken together, these observations indicate that the control of T-cell responses by Arg1 is a common mechanism of immunosuppression in different chronic infectious diseases.

In conclusion, our data demonstrate that Arg1-expressing macrophages in hypoxic and necrotic regions of TB granulomas play a crucial role in controlling both *Mtb* growth and TB pathology, at least in part by restraining T-cell responses, independently of NO production. Hence, our data argue that control of *Mtb* must be balanced regionally with a continuous restriction of T-cell–mediated immunopathology.

Materials and Methods

Ethics Statement. All animal experiments were approved by the local ethics committee of the German authorities, the State Office of Health and Social Affairs Berlin (approval no. G0055/88), and the Animal Care and Use Committee of St. Jude Children's Research Hospital (approval no. 267). Formalin-fixed and paraffin-embedded tissue samples, taken from patients who underwent treatment for tuberculosis at the Central Tuberculosis Research Institute in Moscow were retrieved from the archives of Immunology and Thoracic Surgery, Central Tuberculosis Research Institute. The use of human biopsies as anonymous samples was based on informed patient consent and approved by the ethics commission of Charité — Universitätsmedizin Berlin (61).

Experimental Animals. C57BL/6 (WT) mice were obtained from Charles River Laboratories, *Nos2*$^{-/-}$ (B6.129P2-*Nos2*^{tm1Lau}/J) mice were obtained from the Jackson Laboratory, and *Arg1*$^{flox/flox}$; Tie2-Cre; *Nos2*$^{-/-}$ C57BL/6 mice were bred in our facilities at the Max Planck Institute for Infection Biology, Berlin. Infected mice were maintained at biosafety level 3, under specific pathogen-free conditions.

Infection with *Mtb*. The *Mtb* strain H37Rv (ATCC) was cultured in Middlebrook 7H9 broth (BD) supplemented with 0.05% (vol/vol) Tween 80 and Middlebrook ADC Enrichment (BD) until midlog phase (OD_{600} of 0.6–0.8). Bacteria were harvested, resuspended in PBS, and frozen at –80 °C until use. For dermal infections, mice were anesthetized by i.p. administration of ketamine (65 mg/kg), acepromazine (2 mg/kg), and xylazine (11 mg/kg), and 10^4 *Mtb* in a volume of 20 μL PBS was injected into the ear dermis.

In Vivo Cytokine Blocking. For cytokine blocking, infected *Nos2*$^{-/-}$ mice received 500 μg mAb purified from XMG1.2 (anti–IFN-γ) hybridomas (ATCC) i.p. in PBS on days 14 and 21 p.i. as described previously (37).

Enumeration of cfus. Mice were killed at day 56 p.i., and lungs were removed aseptically and homogenized in 1 mL PBS containing 0.05% Tween 80 (vol/vol). Homogenates were then diluted in PBS containing 0.05% Tween 80 (vol/vol) and were plated onto Middlebrook 7H11 agar plates supplemented with Middlebrook OADC Enrichment (BD). The cfus were enumerated after 3–4 wk of incubation at 37 °C.

Histology. Formalin-fixed and paraffin-embedded tissue samples were taken from patients with TB who underwent selective thoracic surgery at the Department of Thoracic Surgery of the Central Tuberculosis Research Institute, Moscow, Russia.

At the time points described, mice were killed, and lungs were removed aseptically and fixed in PBS containing 4% paraformaldehyde (PFA) (wt/vol) overnight at room temperature. Sections of formalin-fixed, paraffin-embedded tissue (2- to 3-μm thick) were cut, deparaffinized, and subjected to H&E staining (for IHC) or immunostaining (for IF).

For immunostaining, sections were subjected to a heat-induced epitope retrieval step using citrate buffer (pH6) (S2369; Dako) or Target Retrieval Solution (pH9) (S2367; Dako). Slides were rinsed with distilled water, washed in Tris-buffered saline (pH 7.5), and incubated for 1 h at room temperature or overnight at 4 °C with primary antibodies against Arg1 (19/Arginase I: 610708; Becton Dickinson; 1:100), N-20 (sc-18351; Santa Cruz Biotechnology Inc.; 1:100), and H-52 (sc-18351; Santa Cruz Biotechnology Inc.; 1:100) for IHC and against CD3 (A0452; Dako; 1:40), Ki67 antigen (clone TEC-3, M7249; Dako; 1:50), Arg1 (N-20; sc-18351; Santa Cruz Biotechnology Inc.; 1:20), and CD68 (MCA1957T; Abd Serotec; 1:50) for IF. For detection, secondary antibodies donkey anti-rabbit Alexa 488 (711-545-152; Jackson ImmunoResearch; 1:100; excitation at 493 nm, emission at 519 nm), donkey anti-rat Cy3 (712-165-153; Jackson ImmunoResearch; 1:100; excitation at 550 nm, emission at 570 nm), donkey anti-goat Alexa 647 (705-605-147; Jackson ImmunoResearch; 1:100; excitation at 651 nm, emission at 667 nm), biotinylated rabbit anti-rat (312-065-045; Dianova; 1:200), rabbit anti–goat-HRP (305-035-045; Dianova; 1:200), and goat anti–mouse-peroxidase (115-035-166; Jackson ImmunoResearch; 1:1,000) were used for 1 h at room temperature. Peroxidase was detected with diaminobenzidine substrate and the chromogen system (K3467; Dako). Alkaline phosphatase was revealed by Fast Red as a chromogen (K0625; Dako). Nuclei were stained with hematoxylin for IHC and with Hoechst (excitation at 346 nm, emission at 460 nm) for IF. Negative controls were performed by omitting primary antibodies, using corresponding isotypes, and (specifically for Arg1) staining tissue from *Arg1-Nos2* DKO mice. Granuloma hypoxia was evaluated on lung sections using the hypoxia marker PIMO kit Hydroxyprobe-1 (Natural Pharmacia International), according to the manufacturer's instructions.

Microscopy. IHC samples were visualized using a Zeiss AxioImager Z1 microscope equipped with a CCD AxioCam at 25 °C. Images were processed with AxioVision software (Zeiss). IF samples were visualized using a Leica DM R upright epifluorescence microscope at 25 °C. Images were captured using a Nikon DXM1200F camera and Nikon ACT-1 software. Images were processed using Adobe PhotoShop CS3. Granulomas were quantified in H&E-stained sections of the whole left lobe of the lungs. A minimum of 16 individual sections from each mouse in each group ($n = 6$) was used to evaluate total granulomas per section. Caseous granulomas were defined as containing a pink central acellular necrotic region surrounded by a granulomatous inflammatory infiltrate. A minimum of 16 individual sections containing granulomas was evaluated for Arg1 staining per mouse from each group ($n = 6$), and an analogous section was H&E stained

to confirm nonnecrotizing or caseous phenotype. To quantify Ki-67$^+$ and Arg1$^+$ staining in granulomas, an image at 100× magnification was taken to orientate the position of images at 400× magnification that were acquired starting from the center and moving toward the outer limits of the granuloma. Next, in each image at 400× magnification the total number of Ki-67$^+$ cells and the area (in square pixels) of Arg1$^+$ staining were quantified using AutMESS software (Zeiss).

RNA Isolation and Quantitative RT-PCR. For in vivo RNA isolation, lungs were aseptically removed from infected mice at days 28 and 56 p.i. and were homogenized in TRIzol total RNA isolation reagent (Invitrogen). RNA was isolated from TRIzol via chloroform extraction and treatment with ethanol and was dissolved in RNase-free water. RNA was analyzed for quality and quantified using a NanoDrop 1000 Spectrophotometer (Thermo Fischer Scientific). One microgram of total RNA was reverse-transcribed using SuperScript III Reverse Transcriptase (Invitrogen), and 10 ng cDNA was subjected to quantitative RT-PCR using primers for *Arg1* 5′-GGAATCTGCATGGGCAA-CCTGTGT-3′ and 5′AGGGTCTACGTCTCGCAAGCCA-3′. Uptake of SYBR Green (Applied Biosystems) was measured using an ABI PRISM 7900 thermocycler (Applied Biosystems). Cycle threshold values were normalized to those obtained for *GAPDH*, and 2–ΔΔCT was used to calculate change in relative mRNA expression between groups.

Isolation of Lung Leukocytes. Mice were killed, and cells were isolated from lungs of individual mice. Lungs were cut into small pieces and incubated for 30 min at 37 °C in 5% CO_2 in Roswell Park Memorial Institute (RPMI)-10 complete medium (Invitrogen) containing 2 mM L-glutamine, 1 mM sodium pyruvate, 10 mM Hepes buffer, and 10% heat-inactivated FCS supplemented with 0.7 mg/mL blend of collagenase VIII (Sigma), 0.3 mg/mL collagenase D (Roche), and 0.03 mg/mL DNase I (Roche). Lung pieces were pressed through 40-μm cell strainers. Red blood cells were lysed in ammonium chloride buffer, cells were washed with PBS containing 0.2% BSA, and 2×10^6 cells per well were added to 96-well tissue culture plates (Nunc).

Arg1 Intracellular Staining. Cells were blocked with rat serum and αCD16/αCD32 mAb and were surfaced stained with antibodies against CD11b (M1/70; BD Pharmingen), CD11c (HL3; eBioscience), F4/80 (BM8; eBioscience), and Ly6G (1A8; BD Pharmingen). Then cells were fixed with 2% PFA in PBS, permeabilized in saponin buffer, and stained with anti-Arg1 (RandD Systems). From each sample, 50–100,000 leukocyte-gated cells were acquired using a FACS Canto II (BD Pharmingen) and were analyzed using BD FACSDiva and FlowJo software.

Protein Extracts. Lungs were removed aseptically from mice and homogenized in 1 mL tissue lysis buffer containing PBS Tween 20 0.05% (vol/vol) and inhibitors of proteases [Mini cOmplete EDTA-free tablets (Roche)] and phosphatases [PhosSTOP tablets (Roche)]. The homogenate was centrifuged at 14,000 × *g*. Supernatants then were centrifuged in 0.22-μm SPIN-X filter tubes (Corning). Proteins were quantified using the BCA Protein Assay Kit (Thermo Scientific).

Arginase Activity Assay. Arginase activity was determined in protein extracts by measuring the conversion of L-arginine into L-ornithine. In brief, 20 μg of protein was added to 25 μL of 10 mM $MnCl_2$. This mixture was heated at 55–60 °C for 20 min to activate arginase. Then, 150 μL of carbonate buffer (100 mmol/L) (Sigma) and 50 μL of L-arginine (100 mmol/L) (Sigma) were added, and the solution was incubated at 37 °C for 20 min. The hydrolysis reaction from L-arginine to L-ornithine was identified by a colorimetric assay after the addition of ninhydrin solution and incubation at 95 °C for 1 h.

Western Blot. Arg1 (N-20; sc-18351; Santa Cruz Biotechnology) and β-actin (AC-15; ab6276-100; Abcam) expression was detected by immunoblot using 20 μg of protein extracts. Protein extracts were electrophoresed in 12% Tris-Glycine gels (Bio-Rad), transferred to PVDF membranes, and immunoblotted with the appropriate antibodies.

HPLC. Amounts of L-arginine, L-ornithine, putrescine, and spermidine in protein extracts were determined by use of HPLC, as described elsewhere (62). In brief, protein extracts were deproteinized and derivatized, and then each sample was tested. A standard curve with known concentrations of each molecule was run for each experiment.

Evaluation of *Mtb* Growth in the Presence of L-Arginine Metabolites. *Mtb* strain H37Rv (ATCC) was cultured in Middlebrook 7H9 broth (BD) supplemented with 0.05% (vol/vol) Tween 80 and Middlebrook ADC Enrichment (BD) until midlog phase at 37 °C (OD_{600} of 0.6–0.8, corresponding to an approximate cell density of 10^8 cells/mL). Bacteria were harvested by centrifugation, washed with 1× PBS, resuspended in Sauton's medium supplemented with 0.05% (vol/vol) Tween 80, and cultured at 37 °C until reaching an OD_{600} of 0.5. Then, bacteria were cultured at an OD_{600} of 0.05 in Sauton's medium containing serial dilutions of L-arginine (200 μM, 100 μM, 50 μM), L-ornithine (200 μM, 100 μM, 50 μM), putrescine (10 μM, 1 μM, 0.1 μM), spermidine (10 μM, 1 μM, 0.1 μM), and spermine (24 μM, 16 μM, 4 μM). After 1, 2, 4, and 7 d, bacterial growth was evaluated by measurement of OD_{600} and by plating serial dilutions onto Middlebrook 7H11 agar plates and counting the cfus after 3 wk of incubation at 37 °C.

Statistics. Statistical analyses were carried out using Prism 5 software (GraphPad) and the R package nlme (63). Individual comparisons were performed using the Mann–Whitney test. Multiple group comparisons were performed using the Kruskal–Wallis test, followed by Dunn's multiple comparison test to compare individual groups. The association between the number of necrotic and Arg1$^+$ granulomas enumerated in the lungs of infected IFN-γ–blocked *Nos2*$^{-/-}$ mice was estimated by use of a regression model and Spearman's correlation coefficient. Nonparametric tests including the Mann–Whitney test, the Kruskal–Wallis test, and Spearman's correlation were performed when the data were not normal. Accordingly, graphs illustrating these data show the median and the interquartile range. For statistical analysis of the quantification of Ki-67$^+$ cells and the area (in square pixels) of Arg1$^+$ staining in TB lung granulomas, linear models were calculated using the R package nlme (63). The significance of the effects of granuloma type (nonnecrotic or necrotic), presence and absence of Arg1 expression (i.e., mouse strain: *Nos2*$^{-/-}$ and *Arg1-Nos2* DKO mice), and granuloma region and of their interactions was computed using a mixed-effect (type III) linear model (64). In principle, a linear regression model is fitted to each granuloma (with granuloma region as the independent variable and the quantification of the Ki-67$^+$ cells as the dependent variable) and then compares the set of models from granulomas of *Nos2*$^{-/-}$ mice with the set of models from granulomas of *Arg1-Nos2* DKO mice. This technique makes it possible to account for the substantial granuloma-specific variability. For purposes of visualization only (Fig. 5*C*), to account for the granuloma-specific variability, Ki-67 values were centered relative to the value in the first region measured, and a simple linear regression fit was calculated for each combination of granuloma type and mouse strain, separately. All statistical procedures, R code necessary to replicate the results and figures, raw data, and results of statistical analyses are available upon request.

ACKNOWLEDGMENTS. We thank Diane Schad for graphical assistance and Mary Louise Grossman for help in preparing the manuscript. This work was supported by the European Union's Seventh Framework Programme (EU FP7) Collaborative Projects NEWTBVAC (Grant HEALTH-F3-2009-241745), SysteMTb (Grant HEALTH-F4-2010-241587), and (FP7/2007-2013) Grant 280873 ADITEC., CORE Grant P30 CA21765, National Institutes of Health Grant AI097485, The Hartwell Foundation, and The American Lebanese Syrian Associated Charities.

1. Ramakrishnan L (2012) Revisiting the role of the granuloma in tuberculosis. *Nat Rev Immunol* 12(5):352–366.
2. Reece ST, Kaufmann SH (2012) Floating between the poles of pathology and protection: Can we pin down the granuloma in tuberculosis? *Curr Opin Microbiol* 15(1): 63–70.
3. Spector WG (1969) The granulomatous inflammatory exudate. *Int Rev Exp Pathol* 8:1–55.
4. Bold TD, Ernst JD (2009) Who benefits from granulomas, mycobacteria or host? *Cell* 136(1):17–19.
5. Paige C, Bishai WR (2010) Penitentiary or penthouse condo: The tuberculous granuloma from the microbe's point of view. *Cell Microbiol* 12(3):301–309.
6. Russell DG (2007) Who puts the tubercle in tuberculosis? *Nat Rev Microbiol* 5(1):39–47.
7. Dorhoi A, Reece ST, Kaufmann SH (2011) For better or for worse: The immune response against *Mycobacterium tuberculosis* balances pathology and protection. *Immunol Rev* 240(1):235–251.
8. Flynn JL, Chan J, Lin PL (2011) Macrophages and control of granulomatous inflammation in tuberculosis. *Mucosal Immunol* 4(3):271–278.
9. Russell DG, Cardona PJ, Kim MJ, Allain S, Altare F (2009) Foamy macrophages and the progression of the human tuberculosis granuloma. *Nat Immunol* 10(9):943–948.
10. Grohmann U, Bronte V (2010) Control of immune response by amino acid metabolism. *Immunol Rev* 236:243–264.
11. Mattila JT, et al. (2013) Microenvironments in tuberculous granulomas are delineated by distinct populations of macrophage subsets and expression of nitric oxide synthase and arginase isoforms. *J Immunol* 191(2):773–784.

12. Murray PJ, Wynn TA (2011) Protective and pathogenic functions of macrophage subsets. *Nat Rev Immunol* 11(11):723–737.
13. Peranzoni E, et al. (2007) Role of arginine metabolism in immunity and immunopathology. *Immunobiology* 212(9-10):795–812.
14. Fang FC (2004) Antimicrobial reactive oxygen and nitrogen species: Concepts and controversies. *Nat Rev Microbiol* 2(10):820–832.
15. Bogdan C (2001) Nitric oxide and the immune response. *Nat Immunol* 2(10):907–916.
16. Martinez FO, Helming L, Gordon S (2009) Alternative activation of macrophages: An immunologic functional perspective. *Annu Rev Immunol* 27:451–483.
17. Jung YJ, LaCourse R, Ryan L, North RJ (2002) Virulent but not avirulent *Mycobacterium tuberculosis* can evade the growth inhibitory action of a T helper 1-dependent, nitric oxide Synthase 2-independent defense in mice. *J Exp Med* 196(7):991–998.
18. MacMicking JD, et al. (1997) Identification of nitric oxide synthase as a protective locus against tuberculosis. *Proc Natl Acad Sci USA* 94(10):5243–5248.
19. Nathan C (2008) Microbiology. An antibiotic mimics immunity. *Science* 322(5906): 1337–1338.
20. Yang CS, Yuk JM, Jo EK (2009) The role of nitric oxide in mycobacterial infections. *Immune Netw* 9(2):46–52.
21. Ralph AP, Kelly PM, Anstey NM (2008) L-arginine and vitamin D: Novel adjunctive immunotherapies in tuberculosis. *Trends Microbiol* 16(7):336–344.
22. El Kasmi KC, et al. (2008) Toll-like receptor-induced arginase 1 in macrophages thwarts effective immunity against intracellular pathogens. *Nat Immunol* 9(12): 1399–1406.
23. Hart BE, Tapping RI (2012) Differential trafficking of TLR1 I602S underlies host protection against pathogenic mycobacteria. *J Immunol* 189(11):5347–5355.
24. Qualls JE, et al. (2010) Arginine usage in mycobacteria-infected macrophages depends on autocrine-paracrine cytokine signaling. *Sci Signal* 3(135):ra62.
25. Schreiber T, et al. (2009) Autocrine IL-10 induces hallmarks of alternative activation in macrophages and suppresses antituberculosis effector mechanisms without compromising T cell immunity. *J Immunol* 183(2):1301–1312.
26. Heitmann L, et al. (2014) The IL-13/IL-4Rα axis is involved in tuberculosis-associated pathology. *J Pathol*.
27. Bronte V, Zanovello P (2005) Regulation of immune responses by L-arginine metabolism. *Nat Rev Immunol* 5(8):641–654.
28. Rodríguez PC, Ochoa AC (2008) Arginine regulation by myeloid derived suppressor cells and tolerance in cancer: Mechanisms and therapeutic perspectives. *Immunol Rev* 222:180–191.
29. Stempin CC, Dulgerian LR, Garrido VV, Cerban FM (2010) Arginase in parasitic infections: Macrophage activation, immunosuppression, and intracellular signals. *J Biomed Biotechnol* 2010:683485.
30. Pesce JT, et al. (2009) Arginase-1-expressing macrophages suppress Th2 cytokine-driven inflammation and fibrosis. *PLoS Pathog* 5(4):e1000371.
31. Kropf P, et al. (2005) Arginase and polyamine synthesis are key factors in the regulation of experimental leishmaniasis in vivo. *FASEB J* 19(8):1000–1002.
32. Modolell M, et al. (2009) Local suppression of T cell responses by arginase-induced L-arginine depletion in nonhealing leishmaniasis. *PLoS Negl Trop Dis* 3(7):e480.
33. Colotti G, Ilari A (2011) Polyamine metabolism in Leishmania: From arginine to trypanothione. *Amino Acids* 40(2):269–285.
34. Niemand J, Louw AI, Birkholtz L, Kirk K (2012) Polyamine uptake by the intra-erythrocytic malaria parasite, *Plasmodium falciparum*. *Int J Parasitol* 42(10):921–929.
35. Tavares J, Ouaissi A, Lin PK, Tomás A, Cordeiro-da-Silva A (2005) Differential effects of polyamine derivative compounds against *Leishmania infantum* promastigotes and axenic amastigotes. *Int J Parasitol* 35(6):637–646.
36. Esser-von Bieren J, et al. (2013) Antibodies trap tissue migrating helminth larvae and prevent tissue damage by driving IL-4Rα-independent alternative differentiation of macrophages. *PLoS Pathog* 9(11):e1003771.
37. Reece ST, et al. (2010) Serine protease activity contributes to control of *Mycobacterium tuberculosis* in hypoxic lung granulomas in mice. *J Clin Invest* 120(9):3365–3376.
38. Pessanha AP, Martins RA, Mattos-Guaraldi AL, Vianna A, Moreira LO (2012) Arginase-1 expression in granulomas of tuberculosis patients. *FEMS Immunol Med Microbiol* 66(2): 265–268.
39. Lewis JS, Lee JA, Underwood JC, Harris AL, Lewis CE (1999) Macrophage responses to hypoxia: Relevance to disease mechanisms. *J Leukoc Biol* 66(6):889–900.
40. Louis CA, et al. (1998) Distinct arginase isoforms expressed in primary and transformed macrophages: Regulation by oxygen tension. *Am J Physiol* 274(3 Pt 2): R775–R782.
41. Morris CR, et al. (2004) Decreased arginine bioavailability and increased serum arginase activity in asthma. *Am J Respir Crit Care Med* 170(2):148–153.
42. Soda K (2011) The mechanisms by which polyamines accelerate tumor spread. *J Exp Clin Cancer Res* 30:95.
43. Ulrichs T, et al. (2004) Human tuberculous granulomas induce peripheral lymphoid follicle-like structures to orchestrate local host defence in the lung. *J Pathol* 204(2): 217–228.
44. Ulrichs T, Kaufmann SH (2006) New insights into the function of granulomas in human tuberculosis. *J Pathol* 208(2):261–269.
45. Kaplan G, et al. (2003) *Mycobacterium tuberculosis* growth at the cavity surface: A microenvironment with failed immunity. *Infect Immun* 71(12):7099–7108.
46. Elkington PT, D'Armiento JM, Friedland JS (2011) Tuberculosis immunopathology: The neglected role of extracellular matrix destruction. *Sci Transl Med* 3(71):ps6.
47. Murray PJ, Wynn TA (2011) Obstacles and opportunities for understanding macrophage polarization. *J Leukoc Biol* 89(4):557–563.
48. El Kasmi KC, et al. (2014) Adventitial fibroblasts induce a distinct proinflammatory/profibrotic macrophage phenotype in pulmonary hypertension. *J Immunol* 193(2): 597–609.
49. Colegio OR, et al. (2014) Functional polarization of tumour-associated macrophages by tumour-derived lactic acid. *Nature*, 10.1038/nature13490.
50. Obregón-Henao A, Henao-Tamayo M, Orme IM, Ordway DJ (2013) Gr1(int)CD11b+ myeloid-derived suppressor cells in *Mycobacterium tuberculosis* infection. *PLoS ONE* 8(11):e80669.
51. Lin PL, et al. (2014) Sterilization of granulomas is common in active and latent tuberculosis despite within-host variability in bacterial killing. *Nat Med* 20(1):75–79.
52. Meintjes G, et al.; International Network for the Study of HIV-associated IRIS (2008) Tuberculosis-associated immune reconstitution inflammatory syndrome: Case definitions for use in resource-limited settings. *Lancet Infect Dis* 8(8):516–523.
53. Duleu S, et al. (2004) Mouse strain susceptibility to trypanosome infection: An arginase-dependent effect. *J Immunol* 172(10):6298–6303.
54. Gobert AP, et al. (2000) L-Arginine availability modulates local nitric oxide production and parasite killing in experimental trypanosomiasis. *Infect Immun* 68(8):4653–4657.
55. Hesse M, et al. (2001) Differential regulation of nitric oxide synthase-2 and arginase-1 by type 1/type 2 cytokines in vivo: Granulomatous pathology is shaped by the pattern of L-arginine metabolism. *J Immunol* 167(11):6533–6544.
56. Barron L, et al. (2013) Role of arginase 1 from myeloid cells in th2-dominated lung inflammation. *PLoS ONE* 8(4):e61961.
57. Abebe T, et al. (2012) Local increase of arginase activity in lesions of patients with cutaneous leishmaniasis in Ethiopia. *PLoS Negl Trop Dis* 6(6):e1684.
58. Araújo AP, Frezza TF, Allegretti SM, Giorgio S (2010) Hypoxia, hypoxia-inducible factor-1α and vascular endothelial growth factor in a murine model of Schistosoma mansoni infection. *Exp Mol Pathol* 89(3):327–333.
59. Arrais-Silva WW, Paffaro VA, Jr, Yamada AT, Giorgio S (2005) Expression of hypoxia-inducible factor-1alpha in the cutaneous lesions of BALB/c mice infected with Leishmania amazonensis. *Exp Mol Pathol* 78(1):49–54.
60. Herbert DR, et al. (2010) Arginase I suppresses IL-12/IL-23p40-driven intestinal inflammation during acute schistosomiasis. *J Immunol* 184(11):6438–6446.
61. Ulrichs T, et al. (2005) Differential organization of the local immune response in patients with active cavitary tuberculosis or with nonprogressive tuberculoma. *J Infect Dis* 192(1):89–97.
62. Zea AH, et al. (2005) Arginase-producing myeloid suppressor cells in renal cell carcinoma patients: A mechanism of tumor evasion. *Cancer Res* 65(8):3044–3048.
63. Pinheiro J, Bates D, DebRoy S, Sarkar D, and R Development Core Team (2013) nlme: Linear and nonlinear mixed effects models. R package. Version 3.1-109. (R Development Core Team, Vienna).
64. Pinheiro J, Bates D (2000) *Mixed Effects Models in S and S-plus* (Springer, New York), 1st Ed, pp 1–528.